

# Graphene Oxide Thin Films for Flexible Nonvolatile Memory Applications

Hu Young Jeong,<sup>†,♦,○</sup> Jong Yun Kim,<sup>†,§,♦</sup> Jeong Won Kim,<sup>||</sup> Jin Ok Hwang,<sup>†</sup> Ji-Eun Kim,<sup>†</sup> Jeong Yong Lee,<sup>†</sup> Tae Hyun Yoon,<sup>§</sup> Byung Jin Cho,<sup>⊥</sup> Sang Ouk Kim,<sup>†</sup> Rodney S. Ruoff,<sup>#</sup> and Sung-Yool Choi<sup>\*,†,¶</sup>

<sup>†</sup>Department of Materials Science and Engineering, KAIST, Daejeon, 305-701, Korea, <sup>‡</sup>Electronics and Telecommunications Research Institute (ETRI), Daejeon 305-700, Korea, <sup>§</sup>Department of Chemistry, Hanyang University, Seoul, 133-701, Korea, <sup>||</sup>Korea Research Institute of Standards and Science (KRISS), Daejeon, 305-340, Korea, <sup>⊥</sup>Department of Electrical Engineering, KAIST, Daejeon, 305-701, Korea, <sup>#</sup>Department of Mechanical Engineering and the Texas Materials Institute, University of Texas at Austin, Texas, 78712-0292, United States, and <sup>¶</sup>Department of Advanced Device Technology, University of Science and Technology (UST), Daejeon, 305-333, Korea

**ABSTRACT** There has been strong demand for novel nonvolatile memory technology for low-cost, large-area, and low-power flexible electronics applications. Resistive memories based on metal oxide thin films have been extensively studied for application as next-generation nonvolatile memory devices. However, although the metal oxide based resistive memories have several advantages, such as good scalability, low-power consumption, and fast switching speed, their application to large-area flexible substrates has been limited due to their material characteristics and necessity of a high-temperature fabrication process. As a promising nonvolatile memory technology for large-area flexible applications, we present a graphene oxide based memory that can be easily fabricated using a room temperature spin-casting method on flexible substrates and has reliable memory performance in terms of retention and endurance. The microscopic origin of the bipolar resistive switching behavior was elucidated and is attributed to rupture and formation of conducting filaments at the top amorphous interface layer formed between the graphene oxide film and the top Al metal electrode, via high-resolution transmission electron microscopy and in situ X-ray photoemission spectroscopy. This work provides an important step for developing understanding of the fundamental physics of bipolar resistive switching in graphene oxide films, for the application to future flexible electronics.

**KEYWORDS** Graphene oxide, resistive switching, nonvolatile memory, flexible memory, TEM, XPS

The charge-based memory devices such as dynamic random access memory (DRAM) and flash memory, while omnipresent today, do have technological and physical limitations as device dimensions have shrunk. As an alternative, resistive random access memory (RRAM) relying upon a switching mechanism based on change in resistance, has attracted attention as a promising next-generation nonvolatile memory (NVM) owing to its simple structure, facile processing, high density, and fast switching.<sup>1–4</sup> To date, various insulating or semiconducting materials have been found to demonstrate resistive switching, including chalcogenides,<sup>5,6</sup> organic materials,<sup>7,8</sup> amorphous silicon,<sup>9,10</sup> perovskite oxides,<sup>11,12</sup> binary transition metal oxides (such as NiO,<sup>13–15</sup> TiO<sub>2</sub>,<sup>16–18</sup> and ZnO<sup>19</sup>), and even Fe<sub>3</sub>O<sub>4</sub> nanoparticle assemblies.<sup>20</sup>

Fullerenes, carbon nanotubes, and graphene-based materials have attracted attention as future nonvolatile memory elements.<sup>21</sup> Suspended and crossed carbon nanotubes in an array configuration yielded bistable resistance switching

(separation/contact).<sup>22</sup> Two-terminal devices consisting of graphitic sheets grown on nanocables<sup>23</sup> or transferred onto a silicon oxide substrate<sup>24</sup> exhibited an enormous and reversible nonvolatile memory effect, which was attributed to the formation and breaking of carbon atomic chains. Recently, reliable and reproducible resistive switching of graphene oxide (G-O) thin films<sup>25</sup> and conjugated-polymer-functionalized G-O films<sup>26,27</sup> were reported. However, application to flexible substrates has not demonstrated, and also the microscopic origin of resistive switching of thin G-O films is not fully understood.

Here we introduce a nonvolatile flexible memory array based on a G-O thin film. G-O is usually prepared by chemical oxidation of naturally abundant graphite to produce graphite oxide followed by exfoliation of the graphite oxide into individual layers (i.e., graphene oxide or G-O platelets).<sup>28–31</sup> A trilayer Al/G-O film/Al device of cross-point structure was made on flexible polyethersulfone (PES) substrate with a uniform G-O film prepared by spin-casting.<sup>32</sup> This device showed reliable and reproducible bipolar resistive switching (BRS) with an on/off ratio of  $\sim 100$ , a retention time of longer than  $10^5$  s, and switching voltages of  $\sim 2.5$  V. High-resolution transmission electron microscopy (HRTEM) and in situ X-ray photoemission spectroscopy (XPS) measurements showed

\* To whom correspondence should be addressed, sychoi@etri.re.kr.

♦ These authors equally contributed to this work.

○ Current address: Graduate School of EEWS, KAIST, Daejeon, 305-701, Korea.

Received for review: 05/28/2010

Published on Web: 00/00/0000



that the oxygen functional groups decorating the stacked/overlapped G-O platelets in the G-O film migrate into the top interface layer through redox reactions with the top Al electrode during its deposition. The microscopic origin of the BRS behavior is evidently from the formation and depletion of conductive filaments at the top interface layer that arise from reversible diffusion of negatively charged oxygen ions upon the set and reset processes, respectively.

Large-area uniform G-O thin films were made by a simple and scalable spin-casting process. The G-O films are transferrable to any kind of substrate including flexible substrates. The spin-cast G-O thin films can be immediately integrated into practical devices in conjunction with standard CMOS processes so that this approach can be readily used for nonvolatile memory devices. Furthermore, the resistive switching mechanism arising from the interface redox reaction between the Al electrodes and insulating G-O film offers a new paradigm for carbon-based electronics; one can imagine other options such as nonconductive amorphous carbon films that are oxidized on their top surface, and so on.

Graphite oxide was prepared from natural graphite (Graphit Kropfmühl AG, MGR 25 998 K) by a modified Hummers method,<sup>28</sup> and exfoliated into G-O by sonication for 2 h in water.<sup>33</sup> Unexfoliated particles were removed by centrifugation at 15000 rpm for 20 min (Hanil Supra 22 K). The supernatant contained ~2 wt % of G-O. Al/G-O film/Al memory devices were fabricated as follows. Seventy nanometer thick, 50  $\mu\text{m}$  width Al electrode lines were thermally evaporated onto a substrate (PES or  $\text{SiO}_2$ ) through a shadow mask. The Al-patterned substrates were then cleaned with a UV-ozone plasma for 5 min. The aqueous G-O dispersion was spin-cast on the Al-patterned substrate, followed by drying at 120  $^\circ\text{C}$  for 30 min. The thickness and sheet resistance of the spin-cast G-O films were ~15 nm and  $\sim 2 \times 10^4 \Omega/\square$ , respectively. Finally, an Al top electrode of ~70 nm thickness was deposited on the top surface of the G-O film, forming a 5  $\times$  5 cross-bar array memory structure thus having 25 elements, as seen in Figure 1a.

The left inset of Figure 1b is the real photograph of the two-terminal 5  $\times$  5 crossbar memory device with 50  $\mu\text{m}$  line widths on PES substrate. A G-O film (~15 nm thickness) prepared by spin-casting is sandwiched between the top and bottom Al electrodes. Infrared (IR) spectroscopy and Raman spectroscopy confirmed that the as-cast G-O thin film is composed of stacked and overlapped (as also shown by TEM, see below) G-O platelets decorated with oxygen functional groups such as epoxide, hydroxyl, and carboxyl (see Figure S1 in Supporting Information). Highly uniform G-O films without wrinkles were readily prepared on the bottom Al electrodes by spin-casting (see Figures S2 and S5 in Supporting Information). The bottom Al electrode film had a high root mean square value of ~2.5 nm. Perhaps such surface roughness relaxes the stress upon thin film casting,

enabling a large-area processability of a uniform G-O memory device on an Al electrode.

A typical current–voltage ( $I$ – $V$ ) curve of a Al/G-O/Al/PES device as measured with a voltage sweeping mode at room temperature (298 K) is shown in Figure 1b. The voltage bias was applied to the top electrode, and the bottom electrode was grounded. Reversible bistable resistance switching between a high resistance state (HRS) and a low resistance state (LRS) was observed. Unlike typical metal oxide devices, the first negative sweep yielded an “ON” state without any “preforming” procedure.<sup>14–18</sup> As reverse biases are required for switching, our devices represent a typical BRS behavior. Without any optimization of the fabrication process, the device yield of G-O memory cells was higher than 80% (20 successes out of 25 point cells).

In order to confirm the feasibility of our G-O device for flexible memory application,<sup>34</sup> mechanical flexibility tests were measured. When the device was continuously flexed 1000 times, as seen in Figure 1c, the BRS was not degraded. Figure 1d shows the results of a bending test as a function of bending radius ( $R$ ), where the current ratio between the on and off states was maintained until the bending radius reached 7 mm. Because this bending radius can be considered as an “extremely flexed state” (20 mm (flat device)  $\rightarrow$  14 mm), we suggest that this Al/G-O film/Al/PES device is suitable for flexible nonvolatile memory application.

Retention and endurance tests were then conducted. Figure 1e shows the retention behavior of this G-O film flexible memory device. The resistance values of the HRS and the LRS were obtained at a reading voltage of  $-0.5$  V per 600 s after switching each state. Both states showed no disturbance for around  $10^5$  s. The device endurance (Figure 1f) was demonstrated with steady operation for 100 cycles. The resistance values were read out at  $-0.5$  V in each dc sweep. Although the resistance values of both the HRS and LRS showed slight fluctuations, a 100 $\times$  memory window between the ON and OFF state was obtained without any noticeable degradation during the 100 cycles.

The G-O film device had a rapid current increase in the transition region of the negative sweep region. This strongly suggests the formation of conducting filaments.<sup>14,19</sup> The measured  $I$ – $V$  curves were plotted on a double logarithmic plot. The slopes of the  $\log I$ – $\log V$  plot of HRS sequentially changed from 1 to 2 to  $\infty$ , as  $V$  increases for the negative sweep regions (see Figure S3 in Supporting Information). This behavior is qualitatively consistent with the shallow trap-associated space-charge-limited conduction (SCLC) theory, which is generally described by  $I(V) = aV + bV^2$ .<sup>35–38</sup> Other  $I$ – $V$  fitting methods, such as  $\ln(I/T^2)$  vs  $V^{1/2}$  and  $\ln(I/V)$  vs  $V^{1/2}$  revealed that either a Schottky emission or a Pool–Frenkel conduction mechanism can be ruled out (see Figure S4 in the Supporting Information). After a sudden current increase, the device did not follow Ohmic behavior implying the absence of conducting filaments in the bulk G-O thin film. Furthermore, the slope of the  $\log I$ – $\log V$  plot in

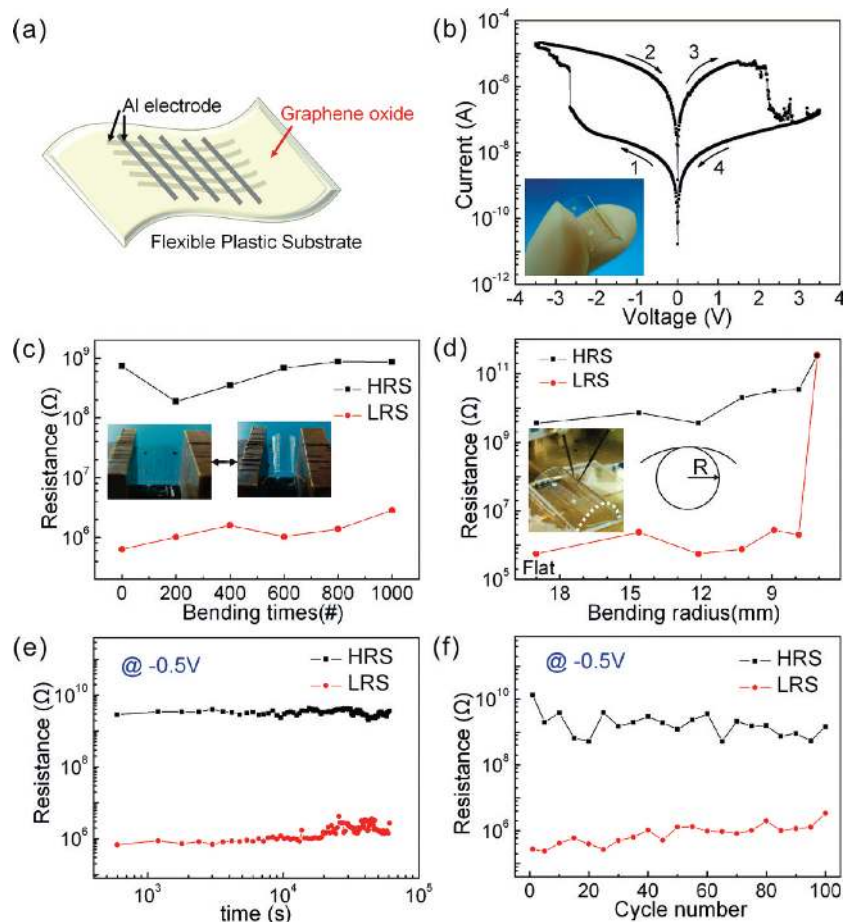


FIGURE 1. (a) A schematic illustration of a G-O based flexible crossbar memory device. (b) Typical  $I-V$  curve of a Al/G-O/Al/PES device plotted on a semilogarithmic scale. The arrows indicate the voltage sweep direction. The left inset is a real photo image of a device. (c) Continuous bending effect of a Al/G-O/Al/PES device. The insets show photographs of repeated two bending states. (d) The resistance ratio between the HRS and LRS as a function of the bending radius ( $R$ ). The inset is a photograph of an  $I-V$  measurement being performed under a flexed condition. (e) Retention test of Al/G-O/Al/PES device read at  $-0.5$  V. (f) Endurance performance of an Al/G-O/Al/PES device measured during 100 sweep cycles.

the high voltage region of the LRS was 1.5 rather than 2; this lower value indicates that the current conduction cannot be simply explained by an electronic trapping and detrapping process as found in other oxide systems.<sup>36,37</sup> We suggest that local filaments are formed and broken in the thin insulating barrier at the interface between the top Al electrode and the G-O thin film, rather than in the bulk G-O film. Such filaments can be induced by oxygen ion transfer between an insulating barrier and G-O top domain.

We have previously reported that a Al/amorphous  $\text{TiO}_2$ /Al RRAM device<sup>39</sup> had a similar BRS behavior as reported here for these Al/G-O film/Al devices. In this earlier study, high-resolution TEM images as well as energy-filtered TEM images showed that the formation (and subsequent dissociation) of an amorphous interface layer (Al-Ti-O) was induced by oxygen ion movement.<sup>40</sup> Because  $\text{TiO}_2$  thin films were grown by plasma-enhanced atomic layer deposition (PEALD), the top interface layer formed by the redox reaction was also homogeneous; oxygen ion movement was uniform under an external bias. In contrast, G-O thin films

deposited by spin-casting are nonhomogenous because they are composed of multiple overlapped and stacked G-O platelets. The top interface insulating barrier is thus nonhomogenous also. This is most likely associated with the abrupt current increase, which is caused by the presence of conducting filaments within the top insulating interface layer, not in the G-O thin film bulk. The intermediate current level of the on state is possible because our G-O film is not a strong insulator but semiconductor, showing a sheet resistance of  $2 \times 10^4 \Omega/\square$ .

X-ray diffraction (XRD) patterns were obtained from G-O film/Al and Al/G-O film/Al samples by the coupled scan method ( $\theta-2\theta$ ) and are shown in Figure 2a. The as-cast G-O thin film with the Al bottom electrode has a peak at  $2\theta = 11.6$  ( $d$ -spacing 7.6 Å), which is in the  $d$ -spacing range of G-O films.<sup>41,42</sup> After the deposition of a 10 nm thick Al top electrode, the intensity of the (002) peak was significantly reduced showing that the structure of the G-O film was influenced by deposition of the top Al metal. In order to further characterize the thin films (Al and G-O

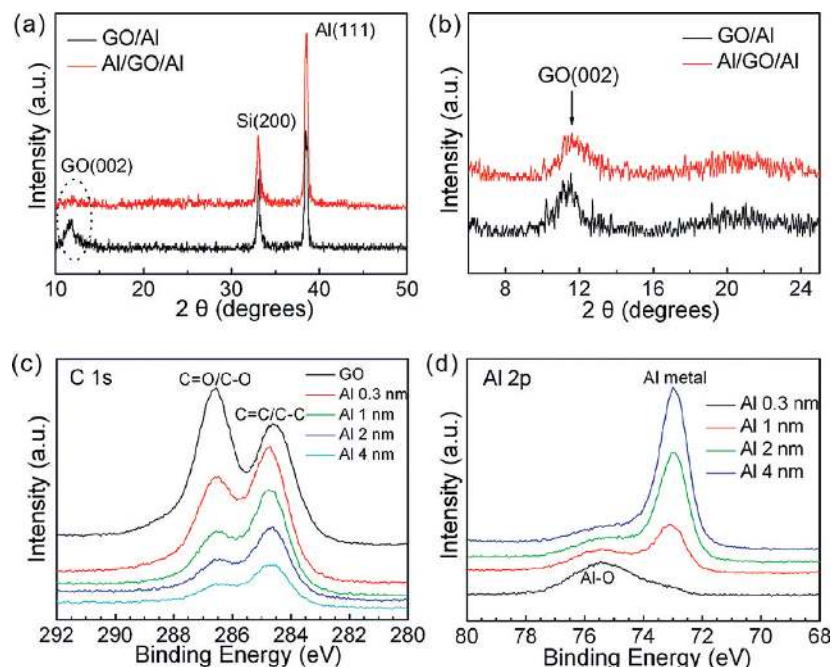


FIGURE 2. XRD patterns of G-O film/Al film and Al film/G-O film/Al film samples measured by (a)  $\theta-2\theta$  coupled and (b) fixed  $\theta$  ( $2^\circ$ ), methods, respectively. In situ XPS spectra of (c) C 1s and (d) Al 2p regions measured as a function of Al thickness.

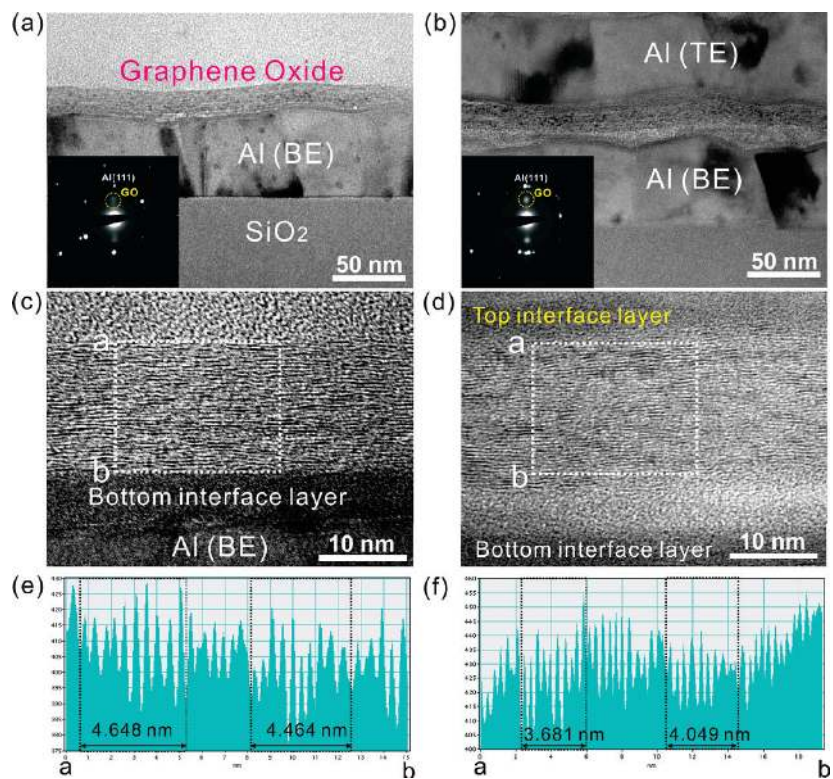


FIGURE 3. Cross-sectional bright field (BF) TEM images of (a) G-O film/Al film and (b) Al film/G-O film/Al film samples. Insets are the SAED patterns measured at the regions containing both G-O film and Al film. HRTEM images of (c) G-O film/Al film and (d) Al film/G-O film/Al film stacks. (e) and (f) are the average profile of intensity obtained in the white rectangular region of (c) and of (d), respectively.

film), XRD patterns were obtained using the fixed  $\theta$  ( $\theta = 2^\circ$ ) method. Figure 2b shows that the  $d$ -spacing of the G-O thin film decreased with increasing Al thickness. It can

be inferred that a reaction between the deposited Al metal and the G-O thin film occurred and that the interlayer distance between platelets in the G-O thin film decreased

due to the loss of oxygen functional groups and the possible expulsion of interlamellar water molecules.

The interfacial chemical reaction between the G-O film and the Al top electrode was characterized by XPS. An in situ XPS measurement was carried out during the growth of continuous ultrathin Al layers on a G-O film. Panels c and d of Figure 2 show the XPS spectra of C 1s and Al 2p measured as a function of Al deposition thickness, respectively. For an as-cast G-O film the C 1s signal is divided into two major peaks: carbon-carbon peak of C=C/C-C in aromatic rings (284.6 eV) related to  $sp^2$  carbon bonding; carbon-oxygen peaks of C-O (286.1 eV), C=O (287.5 eV), and C(=O)-OH (289.2 eV) related to  $sp^3$  carbon bonding.<sup>43</sup> As the Al film thickness increased, the carbon-oxygen bonding peak gradually decreased and eventually its relative intensity with respect to the carbon-carbon peak was significantly diminished—the G-O film surface was strongly reduced upon Al deposition. The Al 2p spectra in Figure 2d show that Al is in the  $Al^{3+}$  oxidation state during the early stages of the Al deposition, demonstrating the formation of an aluminum oxide interface layer. Thus, the surface of the G-O film was reduced while the Al at the interface was oxidized.

The *c* axis stacking in the G-O film was characterized using cross-sectional TEM. Panels a and b of Figure 3 are cross-sectional bright field TEM images obtained before and after the Al top electrode deposition, respectively. The 15 nm thick G-O film was uniformly cast on the Al bottom electrode. The insets are the selective area diffraction patterns (SADP). The strong peaks marked with a white circle correspond to the interlayer lattice for the G-O film. The broad interlayer peak of the pristine G-O film narrowed and was more intense at its maximum after the top Al layer deposition. Panels c and d of Figure 3 are the HRTEM images of the G-O film/Al and Al/G-O film/Al samples, respectively. The bottom interface layer was most likely associated with the native aluminum oxide formed during UV-ozone plasma cleaning (Figure 3c). A top interface layer was formed on the G-O thin film when the top layer of Al was deposited: an amorphous phase with dark contrast as shown in Figure 3d. The average interlayer distances of stacks of G-O platelets (marked with white rectangles) were obtained from the HRTEM intensity profile, as presented in panels e and f of Figure 3. The interlayer spacing was significantly reduced in the Al/G-O film/Al structure. The interlayer spacing near the interface with the top Al film was significantly smaller which further supports the picture of reduction of the G-O film at the interface.

The BRS mechanism of the Al/G-O film/Al device is schematically illustrated in Figure 4. The pristine device has a relatively thick amorphous interface layer due to the redox reaction that occurs at the interface with the Al electrode. This top interface layer is an insulating barrier that dominates the total resistance state (HRS). The critical role of this amorphous layer was also confirmed by replacing the top

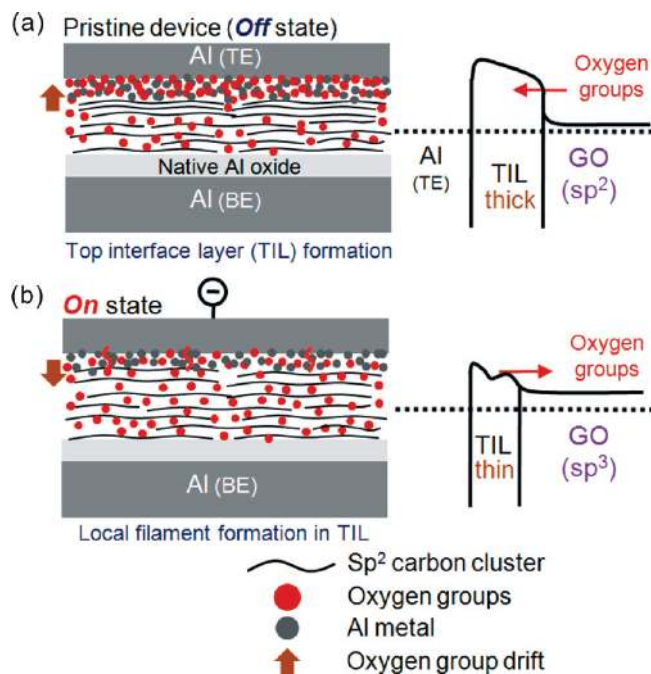


**FIGURE 4.** Schematic of the proposed BRS model for Al electrode/G-O film/Al electrode crossbar memory device. (a) The pristine device is in the OFF state due to the (relatively) thick insulating top interface layer formed by a redox reaction between vapor deposited Al and the G-O film film. (b) The ON state is induced by the formation of local filaments in the top interface layer due to oxygen ion diffusion back into the G-O film film by an external negative bias on the top electrode.

electrode with an inert metal (Au), where the switching behavior was not observed. (see Figure S6a in Supporting Information). With negative bias the device switches into the LRS state due to the growth of local conductive filaments by field-induced oxygen ion diffusion deeper into the G-O film. Because the G-O film below the top interface transformed again to the  $sp^3$ -bonded state and thus did not have conducting filaments, the LRS did not show Ohmic conduction, as shown in Figure 1b. The bottom interface layer (a native aluminum oxide) plays also an important role in protecting the device from an irreversible permanent breakdown, as shown in the case of Au bottom electrode of Figure S6b in Supporting Information.

In summary, we have demonstrated that uniform G-O thin films prepared by simple spin-casting can be successfully utilized in a novel nonvolatile flexible crossbar memory device. This device exhibited a typical BRS with set/reset voltage of  $\sim -2.5$  V /  $+2.5$  V and a high ON/OFF ratio of  $>10^2$ . Both ON and OFF states were stable for more than  $10^5$  s after removal of the external voltage stimulus. No degradation of memory performance was observed  $\sim 100$  cycles. The microscopic origin of the BRS in such Al/G-O film/Al devices is probably due to the formation and rupture of conducting filaments in the insulating barrier at the top interface, not throughout the entire G-O bulk film. The reduction at the interface of the G-O film and oxidation of the top Al electrode

at the same interface were demonstrated by XRD, in situ XPS, and HRTEM.

**Acknowledgment.** This work was supported by the basic research program of ETRI (10ZE1160) sponsored by the Korean Research Council for Industrial Science and Technology, the national program for the next-generation nonvolatile memory of MKE (10029953-2009-31), and the pioneer research central program (2009-0093758, NRF, MEST). S. O. Kim acknowledges financial support from National Research Laboratory Program (R0A-2008-000-20057-0, NRF, MEST).

**Supporting Information Available.** Figures showing FT-IR transmittance and Raman spectra of G-O film, FE-SEM and AFM images of G-O film, typical  $I-V$  curves of Al/G-O/Al/SiO<sub>2</sub> device, Schottky plots of  $I-V$  curves, cross-sectional BF-TEM images, and  $I-V$  characteristics of Au/G-O film/Al and Al/G-O film/Au devices. This material is available free of charge via the Internet at <http://pubs.acs.org>.

## REFERENCES AND NOTES

- Meijer, G. I. *Science* **2008**, *319*, 1625–1626.
- Waser, R.; Aono, M. *Nat. Mater.* **2007**, *6*, 833–840.
- Sawa, A. *Mater. Today* **2008**, *11*, 28–36.
- Waser, R.; Dittmann, R.; Staikov, G.; Szot, K. *Adv. Mater.* **2009**, *21*, 2632–2663.
- Wuttig, M. *Nat. Mater.* **2005**, *4*, 265–266.
- Lankhorst, M. H. R.; Ketelaars, B. W. S. M. M.; Wolters, R. A. M. *Nat. Mater.* **2005**, *4*, 347.
- Ouyang, J.; Chu, C.-W.; Szmanda, C. R.; Ma, L.; Yang, Y. *Nat. Mater.* **2004**, *3*, 918–922.
- Scott, J. C.; Bozano, L. D. *Adv. Mater.* **2007**, *19*, 1452–1463.
- Jo, S. H.; Lu, W. *Nano Lett.* **2008**, *8*, 392–397.
- Jo, S. H.; Kim, K.-H.; Lu, W. *Nano Lett.* **2009**, *9*, 870–874.
- Asamitsu, A.; Tomioka, Y.; Kuwahara, H.; Tokura, Y. *Nature* **1997**, *388*, 50–52.
- Szot, K.; Speier, W.; Bihlmayer, G.; Waser, R. *Nat. Mater.* **2006**, *5*, 312–320.
- Baek, I. G.; Lee, M. S.; Seo, S.; Lee, M. J.; Seo, D. H.; Suh, D.-S.; Park, J. C.; Park, S. O.; Kim, H. S.; Yoo, I. K.; Chung, U.-I.; Moon, J. T. *Tech. Dig.—Int. Electron Devices Meet.* **2004**, 587–590.
- Lee, M.-J.; Han, S.; Jeon, S. H.; Park, B. H.; Kang, B. S.; Ahn, S.-E.; Kim, K. H.; Lee, C. B.; Kim, C. J.; Yoo, I.-K.; Seo, D. H.; Li, X.-S.; Park, J.-B.; Lee, J.-H.; Park, Y. *Nano Lett.* **2009**, *9*, 1476–1481.
- Lee, M.-J.; Kim, S. I.; Lee, C. B.; Yin, H.; Ahn, S.-E.; Kang, B. S.; Kim, K. H.; Park, J. C.; Kim, C. J.; Song, I.; Kim, S. W.; Stefanovich, G.; Lee, J. H.; Chung, S. J.; Kim, Y. H.; Park, Y. *Adv. Funct. Mater.* **2009**, *19*, 1587–1593.
- Yang, J. J.; Pickett, M. D.; Li, X.; Ohlberg, D. A. A.; Stewart, D. R.; Williams, R. S. *Nat. Mater.* **2008**, *7*, 429–433.
- Yang, J. J.; Miao, F.; Pickett, M. D.; Ohlberg, D. A. A.; Stewart, D. R.; Lau, C. N.; Williams, R. S. *Nanotechnology* **2009**, *20*, 215201.
- Yang, J. J.; Borghetti, J.; Murphy, D.; Stewart, D. R.; Williams, R. S. *Adv. Mater.* **2009**, *21*, 3754–3758.
- Yang, Y. C.; Pan, F.; Liu, Q.; Liu, M.; Zeng, F. *Nano Lett.* **2009**, *9*, 1636–1645.
- Kim, T. H.; Jang, E. Y.; Lee, D. J.; Lee, K.-J.; Jang, J.-T.; Choi, J.-S.; Moon, S. H.; Cheon, J. *Nano Lett.* **2009**, *9*, 2229–2233.
- Krepl, F.; Bruchhaus, R.; Majewski, P.; Philipp, J. B.; Symanczyk, R.; Happ, T.; Arndt, C.; Vogt, M.; Zimmermann, R.; Buerke, A.; Graham, A. P.; Kund, M. *Proc.—IEEE Electron Devices Meet.* **2008**, 521–524.
- Rueckes, T.; Kim, K.; Joselevich, E.; Tseng, G. Y.; Cheung, C.-L.; Lieber, C. M. *Science* **2000**, *289*, 94–97.
- Li, Y.; Sinitskii, A.; Tour, J. M. *Nat. Mater.* **2008**, *7*, 966–971.
- Standley, B.; Bao, W.; Zhang, H.; Bruck, J.; Lau, C. N.; Bockrath, M. *Nano Lett.* **2008**, *8*, 3345–3349.
- He, C. L.; Zhuge, F.; Zhou, X. F.; Li, M.; Zhou, G. C.; Liu, Y. W.; Wang, J. Z.; Chen, B.; Su, W. J.; Liu, Z. P.; Wu, Y. H.; Cui, P.; Li, R.-W. *Appl. Phys. Lett.* **2009**, *95*, 232101.
- Zhuang, X.-D.; Chen, Y.; Liu, G.; Li, P.-P.; Zhu, C.-X.; Kang, E.-T.; Noeh, K.-G.; Zhang, B.; Zhu, J.-H.; Li, Y.-X. *Adv. Mater.* **2009**, *22*, 1731–1735.
- Liu, G.; Zhuang, X.; Chen, Y.; Zhang, B.; Zhu, J.; Zhu, C.-X.; Neoh, K.-G.; Kang, E.-T. *Appl. Phys. Lett.* **2009**, *95*, 253301.
- Park, S.; Ruoff, R. S. *Nat. Nanotechnol.* **2009**, *4*, 217–224.
- Stankovich, S.; Dikin, D. A.; Dommett, G. H. B.; Kohlhaas, K. M.; Zimney, E. J.; Stach, E. A.; Piner, R. D.; Nguyen, S. T.; Ruoff, R. S. *Nature* **2006**, *442*, 282–286.
- Dikin, D. A.; Stankovich, S.; Zimney, E. J.; Piner, R. D.; Dommett, G. H. B.; Evmenenko, G.; Nguyen, S. T.; Ruoff, R. S. *Nature* **2007**, *448*, 457–460.
- Watcharotone, S.; Dikin, D. A.; Stankovich, S.; Piner, R.; Jung, I.; Dommett, G. H. B.; Evmenenko, G.; Wu, S.-E.; Chen, S.-F.; Liu, C.-P.; Nguyen, S. T.; Ruoff, R. S. *Nano Lett.* **2007**, *7*, 1888–1892.
- Lee, D. H.; Kim, J. E.; Han, T. H.; Hwang, J. W.; Jeon, S. W.; Choi, S.-Y.; Hong, S. H.; Lee, W. J.; Ruoff, R. S.; Kim, S. O. *Adv. Mater.* **2010**, *22*, 1247–1252.
- Han, T. H.; Lee, W. J.; Lee, D. H.; Kim, J. E.; Choi, E.-Y.; Kim, S. O. *Adv. Mater.* **2010**, *22*, 2060–2064.
- Jeong, H. Y.; Kim, Y. I.; Lee, J. Y.; Choi, S.-Y. *Nanotechnology* **2010**, *21*, 115205.
- Rose, A. *Phys. Rev.* **1955**, *6*, 1538–1544.
- Lee, H.-S.; Bain, J. A.; Choi, S.; Salvador, P. A. *Appl. Phys. Lett.* **2007**, *90*, 202107.
- Choi, H.; Jung, H.; Lee, J.; Yoon, J.; Park, J.; Seong, D.-J.; Lee, W.; Hasan, M.; Jung, G.-Y.; Hwang, H. *Nanotechnology* **2009**, *20*, 345201.
- Dong, R.; Lee, D. S.; Xiang, W. F.; Oh, S. J.; Seong, D. J.; Heo, S. H.; Choi, H. J.; Kwon, M. J.; Seo, S. N.; Pyun, M. B.; Hasan, M.; Hwang, H. *Appl. Phys. Lett.* **2007**, *90*, No. 042107.
- Jeong, H. Y.; Lee, J. Y.; Ryu, M.-K.; Choi, S.-Y. *Phys. Status Solidi RRL* **2010**, *4*, 28–30.
- Jeong, H. Y.; Lee, J. Y.; Choi, S.-Y.; Kim, J. W. *Appl. Phys. Lett.* **2009**, *95*, 162108.
- Jeong, H.-K.; Lee, Y. P.; Lahaye, R. J. W. E.; Park, M.-H.; An, K. H.; Kim, I. J.; Yang, C.-W.; Park, C. Y.; Ruoff, R. S.; Lee, Y. H. *J. Am. Chem. Soc.* **2008**, *130*, 1362–1366.
- McAllister, M. J.; Li, J.-L.; Adamson, D. H.; Schniepp, H. C.; Abdala, A. A.; Liu, J.; Herrera-alonso, M.; Millius, D. L.; Car, R.; Prud'homme, R. K.; Aksay, I. A. *Chem. Mater.* **2007**, *19*, 4396–4404.
- Mattevi, C.; Eda, G.; Agnoli, S.; Miller, S.; Mkhoyan, K. A.; Celik, O.; Mastrogianni, D.; Granozzi, G.; Garfunkel, E.; Chhowalla, M. *Adv. Funct. Mater.* **2009**, *19*, 2577–2583.